

## The Effect of Carbon Emission Trend on Urban Thermal Environment from the Perspective of Transportation Energy Consumption



Shouhui He<sup>1\*</sup>, Hongda Liu<sup>2</sup>, Yan Wang<sup>3</sup>

<sup>1</sup> School of Logistics, Linyi University, Linyi 276000, China

<sup>2</sup> People's Political Consultative Conference of Fei Country, Linyi 276000, China

<sup>3</sup> Linyi Zhixing Traffic Planning & Design Co., LTD, Linyi 276000, China

Corresponding Author Email: [supremehe@163.com](mailto:supremehe@163.com)

<https://doi.org/10.18280/ijht.400424>

### ABSTRACT

**Received:** 28 April 2022

**Accepted:** 30 June 2022

#### Keywords:

*transportation energy consumption, carbon emission, urban thermal environment, urban heat island (UHI) effect*

Figuring out the action mechanism of carbon emission trend on the influencing factors of urban thermal environment from the perspective of transportation energy consumption is of great significance for transforming citizens' means of transportation and promoting sustainable development of urban environment. However, existing studies on urban thermal environment generally focus on the quantification of urban landscape forms, the correlation analysis, or the analysis of relative importance, few of them have concerned about the action mechanism of fluid flow, heat transfer, pollutant diffusion and other process parameters on the Urban Heat Island (UHI) effect with both transportation energy consumption and carbon emission trend taken into consideration. For this reason, this paper gave the spatial structure of urban thermal environment, constructed fluid flow control equation, heat transfer control equation, pollutant diffusion control equation, and turbulence model for the urban thermal environment; then, it quantitatively analyzed the UHI intensity and air pollutant concentration, aiming to alleviate the UHI effect under the influence of transportation energy consumption and carbon emission trend. At last, this paper used experimental results to verify the effectiveness of the constructed model and gave the analysis results of thermal environment in the target city.

## 1. INTRODUCTION

For developed countries that have completed industrialization, the carbon emission from the transportation field accounts for about one third of the total carbon emission [1-4]. In China, the transportation energy consumption accounts for more than 15% of all terminal energy consumption, and the carbon emission from the transportation field accounts for 10.4% of the total carbon emission [5-14]. When exploring the UHI effect, transportation energy consumption and carbon emission are important factors that cannot be ignored, there's a close connection between urban thermal environment and transportation carbon emission [15, 16]. In a background that the carbon peaking and carbon neutrality policies are being implemented in China, transportation carbon emission has been effectively controlled, and the UHI effect has been alleviated as well [17-21]. For China, to achieve the goals of reaching CO<sub>2</sub> emission peak before 2030 and realizing carbon neutralization before 2060, it is very important to figure out the action mechanism of carbon emission trend on the influencing factors of urban thermal environment from the perspective of transportation energy consumption so as to transform citizens' means of transportation and promote sustainable development of urban environment.

Vehicle heat is a kind of man-made heat that can affect the urban thermal environment, the quantification of vehicle heat can affect the potential benefit of electric vehicles in the city, but the study on the spatial and temporal effects of vehicle heat

is insufficient. Li and He [22] incorporated very high frequency and urban landscape data into a weather research and forecasting model and used fine spatial resolution to estimate the very high frequency effect of Hong Kong, the results showed that the vehicle heat exhibited significant temporal changes on daily, weekly, and seasonal scales; the temporal and spatial distribution of vehicle heat effect offers suggestions for the potential benefit of green transportation technology and policy in alleviating the UHI effect. As the urbanization progress is accelerating in China, the urban ground thermal environment has undergone great changes, which is closely related to urban ecological security, social economic activity, and the comfort and health of residents, Chen et al. [23] adopted the spatial regression method to quantify the correlation between urban ground thermal environment and the multi-center structure of prefecture-level and above major cities in China in 2015, 2010 and 2003, and the results showed that there's no significant correlation between the multi-center structure of the city and the average land surface temperature. Now urban agglomerations are facing the problem of regional thermal environment deterioration, but the relationship between the changes in the thermal environment of urban agglomerations and the driving mechanism of urban forms is not clear to us, therefore, Zhang et al. [24] quantified the urban landscape forms and analyzed the correlation and relative importance based on the data of three major urban agglomerations in China in 2000, 2010 and 2020, discussed the responses of regional heat island changes to the urban form changes caused by city expansion, and the

results suggested obvious temporal and spatial consistency in the distribution of heat source and building area in urban agglomerations. Understanding the temporal and spatial patterns of urban heat island and its influencing factors can help reduce the thermal pressure of urban warming and strengthen the city's ability to resist heat-related disasters, thereby contributing to realizing sustainable development. Baqa et al. [25] studied the changes in the land use and land cover of the tropical megacity Karachi in Pakistan and its impact on the urban thermal environment, the writers plotted land cover maps and used satellite images of the land during 2000 and 2020 to estimate the land surface temperature and quantify the surface UHI intensity.

After reviewing relevant literatures, it's found that existing studies on urban thermal environment generally focus on the quantification of urban landscape forms, the correlation analysis, or the analysis of relative importance; and foreign studies on transportation energy consumption and carbon emission trend mostly talk about the carbon emission structure or the use of clean energy in transportation tools, few of them have concerned about the action mechanism of fluid flow, heat transfer, pollutant diffusion and other process parameters on the UHI effect with both transportation energy consumption and carbon emission trend taken into consideration. Therefore, this paper studied the urban thermal environment under the influence of transportation energy consumption and carbon emission trend. In the second chapter, this paper gave the spatial structure of urban thermal environment, constructed fluid flow control equation, heat transfer control equation, pollutant diffusion control equation, and turbulence model for the urban thermal environment. In the third chapter, this paper

quantitatively analyzed the UHI intensity and air pollutant concentration, aiming to alleviate the UHI effect under the influence of transportation energy consumption and carbon emission trend. At last, this paper used experimental results to verify the effectiveness of the constructed model and gave the analysis results of the thermal environment in the target city.

## 2. MODELLING OF URBAN THERMAL ENVIRONMENT

Figure 1 shows the spatial structure of urban thermal environment affected by the heat and pollutants generated from activities in the city. In this paper, the thickness of the atmospheric boundary layer is defined as the height of the mixed layer of the city. Due to the effects of traffic flow, temperature difference between day and night, and solar radiation, there are certain differences in the height of the mixed layer at different times of a day, and a new cycle starts from the beginning of each day. Figure 2 gives the changes in the height of the mixed layer at different times of a day.

To figure out the change mechanism of urban thermal environment under the effects of transportation energy consumption and carbon emission trend, at first, this paper built a primary control equation for the fluid simulation calculation in the urban thermal environment. The research contents of this paper included the fluid flow, temperature distribution, and pollutant diffusion in the urban thermal environment, so the constructed model contained the fluid flow control equation, the heat transfer control equation, the pollutant diffusion control equation, and the turbulence model.

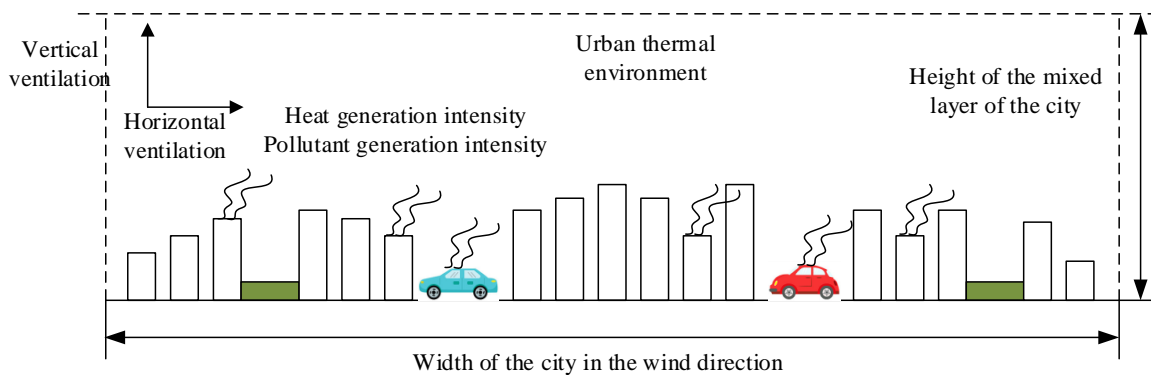


Figure 1. Spatial structure of urban thermal environment

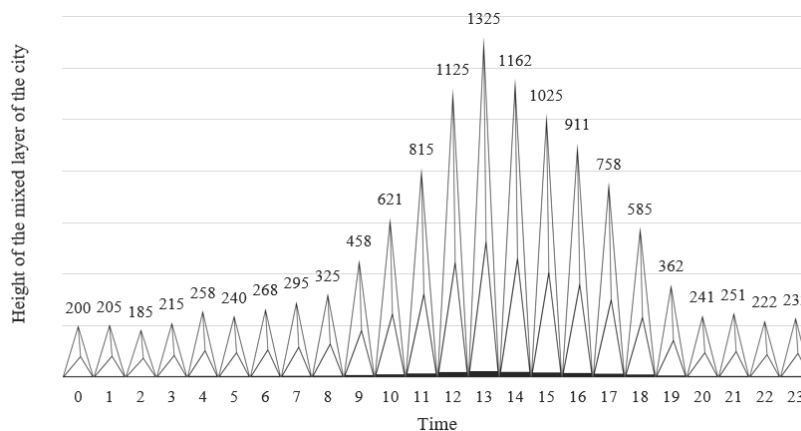


Figure 2. Changes in the height of the mixed layer at different times of a day

Assuming:  $e$  represents the time;  $v'_i$  and  $v'_j$  respectively represent the velocity component of the urban thermal environment fluid in three directions of a, b, and c;  $\sigma$  represents the density of the fluid;  $GS'$  represents the average pressure of the fluid;  $\lambda$  and  $\lambda_e$  respectively represent the dynamic viscosity coefficient and the turbulent dynamic viscosity coefficient;  $\alpha$  represents the thermal expansion coefficient;  $E'$  represents the average temperature of the fluid;  $\beta$  and  $\beta_e$  respectively represent the thermal diffusion rate and the turbulent thermal diffusion rate;  $R_i$  represents the additional term of momentum source;  $Pr_t$  represents the turbulent Prandtl number, then there is  $\beta_e = \lambda_e / Pr_t$ . Based on the conservation law of mass, there is:

$$\frac{\partial \sigma}{\partial e} + \frac{\partial (\sigma v'_i)}{\partial a_i} = 0 \quad (1)$$

Based on the conservation law of momentum, there is:

$$\frac{\partial (\sigma v'_i)}{\partial e} + \frac{\partial (\sigma v'_i v'_j)}{\partial a_j} = -\frac{\partial GS'}{\partial a_i} + \frac{\partial}{\partial a_j} \left( \lambda \frac{\partial v'_i}{\partial a_j} \right) + R_i \quad (2)$$

Based on the conservation law of energy, there is:

$$\frac{\partial E'}{\partial e} + \frac{\partial (v'_j E')}{\partial a_j} = -\frac{\partial}{\partial a_j} (\beta + \beta_e) \frac{\partial E'}{\partial a_j} \quad (3)$$

To reduce the huge computation load required for directly solving the control equation, the RANS (Reynolds Average Navier-Stokes) simulation method could be adopted to realize the time-average characterization of the transient pulsating quantity. Assuming:  $\Psi'$  represents the average value of time;  $\Psi$  represents the instantaneous value;  $\Psi''$  represents the impulse value, then the following formula gives the time-average processing of any variable  $\Psi$  using RANS:

$$\Psi' = \frac{1}{\Delta e} \int_e^{e+\Delta e} \Psi(e) de \quad (4)$$

$$\Psi = \Psi' + \Psi'' \quad (5)$$

Assuming:  $\sigma(v''_i v''_j)^*$  represents the turbulent stress of the urban thermal environment fluid, based on the concept of time-average, the mass conservation equation is given by the following formula:

$$\frac{\partial \sigma}{\partial e} + \frac{\partial v'_i}{\partial a_i} = 0 \quad (6)$$

The following formula gives the corresponding momentum conservation equation:

$$\begin{aligned} \sigma \frac{\partial v'_i}{\partial e} + \frac{\partial}{\partial a_i} (\sigma v'_i v'_j) &= -\frac{\partial GS'}{\partial a_i} \\ + \frac{\partial}{\partial a_j} \left( \lambda \frac{\partial v'_i}{\partial a_j} \right) &+ \frac{\partial}{\partial a_j} (\sigma (v''_i v''_j)^*) + R_i \end{aligned} \quad (7)$$

In order to avoid to directly process the Reynolds stress term, this paper compiled it into a turbulent viscosity function and built a turbulent viscosity model. Based on the eddy viscosity

assumption, the Reynolds stress term was described in the form of average velocity gradient, then there is:

$$-\overline{\sigma v'_i v'_j} = \lambda_t \left( \frac{\partial \bar{v}_i}{\partial a_j} + \frac{\partial \bar{v}_j}{\partial a_i} \right) - \frac{2}{3} \left( \sigma l + \lambda_e \frac{\partial \bar{v}_i}{\partial a_i} \right) \xi_{ij} \quad (8)$$

Assuming:  $\lambda_e$  represents the turbulent viscosity;  $v'_i$  and  $v'_j$  represent the time-average flow velocity;  $\xi_{ij}$  is a binary function, and it satisfies that when  $i=j$ ,  $\xi_{ij}$  is  $k$ ; when  $i \neq j$ ,  $\xi_{ij}$  is 0;  $l$  represents the turbulent impulse kinetic-energy, and it satisfies  $l = 1/2 (v''_i v''_i)^* = 1/2 [(v''^2)^* + (u''^2)^* + (q''^2)^*]$ .

The key in turbulence calculation is to attain accurate  $\lambda_e$ . Assuming  $\rho$  represents the dissipation rate of turbulent impulse kinetic-energy, then  $\lambda_e$  can be calculated by the following formula:

$$\lambda_e = \sigma Z_\lambda \frac{l^2}{\rho} \quad (9)$$

The simulation of all hot air flow fields in the urban thermal environment was carried out by the *standard k-ε* model optimized based on the RNG differential formula so that the high strain gradient and the trace curvature of the hot air flow fields were effectively processed. Assuming  $H_i$  represents the turbulent kinetic-energy generation term;  $H_y$  represents the buoyancy force generation term;  $\varepsilon_i$  and  $\varepsilon_\rho$  respectively represent the Prandtl number of the turbulent kinetic-energy and its dissipation rate;  $Z_{1\rho}$  and  $Z_{2\rho}$  represent empirical constants, then the model could be expressed as:

$$\begin{aligned} \frac{\partial}{\partial e} (\sigma l) + \frac{\partial}{\partial a_i} (\sigma l v'_i) &= \\ \frac{\partial}{\partial a_j} \left( \left( \lambda + \frac{\lambda_e}{\varepsilon_i} \right) \frac{\partial l}{\partial a_j} \right) &+ H_i + H_y - \sigma \rho \end{aligned} \quad (10)$$

$$\begin{aligned} \frac{\partial}{\partial e} (\sigma \rho) + \frac{\partial}{\partial a_i} (\sigma \rho v'_i) &= \frac{\partial}{\partial a_i} \left( \left( \lambda + \frac{\lambda_e}{\varepsilon_\rho} \right) \frac{\partial \rho}{\partial a_j} \right) \\ + Z_{1\rho} \frac{\rho}{l} (H_i + H_y) - Z_{2\rho} \sigma \frac{\rho}{l} \end{aligned} \quad (11)$$

The calculation formula of the model constant is:

$$Z_{1\rho}(\Phi) = 1.42 - \left( \frac{\Phi \left( 1 - \frac{\Phi}{4.38} \right)}{1 + 0.012\Phi^3} \right), \Phi = \frac{LR}{\rho}, R = (R_{ij} R_{ij})^{\frac{1}{2}} \quad (12)$$

For the algorithm that simulates the diffusion of dust particles during the process of transportation energy consumption and carbon emission, the Lagrange model that has obvious advantages in unsteady state calculation had been adopted to give accurate descriptions to the overall spatial distribution of the dust particles. Assuming:  $v'_o$  represents the velocity of dust particles;  $v'_x$  represents the velocity of continuous phase;  $G_C(v'_x - v'_o)$  represents the drag force for per unit mass;  $\sigma_o$  represents the density of dust particles;  $\sigma_x$  represents the density of continuous phase;  $G'_x$  represents the external force of dust particles;  $h'$  represents the acceleration

of gravity, then the following formula gives the expression of the model:

$$\frac{dv'_o}{de} = G_c (\bar{v}'_e - \bar{v}'_o) + \frac{h'(\sigma'_x - \sigma'_o)}{\sigma'_o} + G'_x \quad (13)$$

Assuming:  $\lambda$  represents the air viscosity;  $c_o$  represents the diameter of dust particles;  $Z_z$  represents the correction factor of the diameter of dust particles, then the drag force is:

$$G_{DF} = G_c (v'_x - v'_o) = \frac{18\lambda}{\sigma'_o c_o^2 Z_z} (v'_x - v'_o) \quad (14)$$

The effect of the Saffman lift force on the movement of the dust particles had been fully considered, then the following formula gives the discrete phase equation for the diffusion of dust particles:

$$\frac{d\bar{v}'_o}{de} = G_c (\bar{v}'_x - \bar{v}'_o) + \frac{\bar{h}(\sigma'_o - \sigma'_x)}{\sigma'_o} + \bar{G}_R \quad (15)$$

### 3. UHI INTENSITY AND AIR POLLUTANT CONCENTRATION

In order to alleviate the UHI effect under the influence of transportation energy consumption and carbon emission trend, and reduce the air pollution caused by transportation, it's necessary to quantitatively analyze the UHI intensity and the air pollutant concentration.

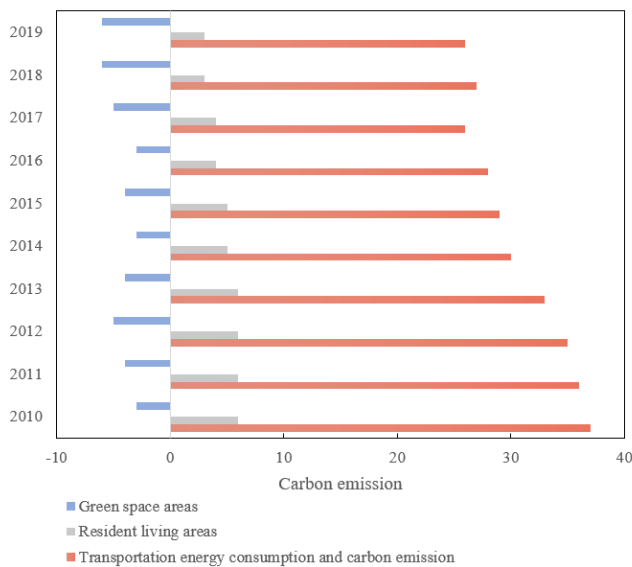


**Figure 3.** Changes of carbon emission of various types of land areas in a city

The UHI intensity was measured based on the difference between the environment temperature in the downtown of the city and the environment temperature of the suburbs, the main influencing factors of this temperature difference were summarized into several aspects, including the population density, transportation energy consumption and carbon emission, planning and layout of urban land types, and the underlying surface characteristics of urban land, etc. Figure 3

gives the changes in the carbon emission of each land type in the city. As can be seen from the figure, compared with the energy consumption and carbon emission of resident living areas, the heat generated by transportation energy consumption and carbon emission was higher, accounting for the vast majority of the total heat.

Assuming:  $E_v(^{\circ}C)$  represents the environment temperature in the downtown;  $E_s(^{\circ}C)$  represents the environment temperature in the suburb;  $\phi$  and  $r$  represent the air density and constant-pressure specific heat in the urban space;  $W_f$  represents the intensity of the heat generated by transportation energy consumption and carbon emission;  $K$  represents the length of the city along the wind flow direction;  $Q$  represents the length of the city in the vertical wind direction;  $V$  represents the average wind speed in the mixed layer of the city;  $\theta$  represents the height of the mixed layer, then, based on the law of mass conservation, in the environment of the city, within unit time and unit volume, there is:

$$\phi r (E_v - E_s) = \frac{W_f \cdot K \cdot Q}{V \cdot \theta \cdot Q} \quad (16)$$

Defining:  $HII$  represents the UHI intensity and it satisfies  $HII = E_v - E_s$ , that is:

$$HII = \frac{W_f \cdot K}{\phi \cdot r \cdot V \cdot \theta} \quad (17)$$

According to above formula, UHI intensity is directly related to the heat dissipation intensity of the typical urban heat source (namely transportation energy consumption and carbon emission) and other parameters of  $K$ ,  $Q$ ,  $V$ ,  $\theta$ ,  $\phi$ , and  $r$ ; UHI intensity is directly proportional to  $K$  and inversely proportional to  $V$ ,  $\theta$ ,  $\phi$ , and  $r$ .

The energy consumption of industry, transportation, and resident living can produce many types of air pollutants to the environment in the city, especially the transportation energy consumption and carbon emission that are closer to the living of the citizens, and they can cause great harm to the urban thermal environment and the health of human body. In this paper, the concentration of inhalable particulate matter  $PM_{10}$  with a particle size less than 10 microns produced from vehicle exhaust, and the concentrations of  $SO_2$  and  $NO_2$  were determined as the main indicators for measuring the air pollution in the city. Assuming:  $ND_o$  represents the concentration of air pollutants in the city;  $WD_o$  represents the intensity of pollutants produced in the city, based on the law of mass conservation, in the environment of the city, within unit time and unit volume, there is:

$$ND_o \cdot V \cdot \theta \cdot W = W_o \cdot K \cdot W \quad (18)$$

The calculation formula of  $ND_o$  is:

$$ND_o = \frac{W_o \cdot K}{V \cdot \theta} \quad (19)$$

According to above formula, the urban air pollutant concentration is directly related to the pollutants dissipated from transportation energy consumption, and other parameters of  $K$ ,  $V$ , and  $\theta$ ; it is directly proportional to  $K$  and inversely proportional to  $V$ , and  $\theta$ .

#### 4. EXPERIMENTAL RESULTS AND ANALYSIS

In this study, the daily changes of the UHI intensity of the target city were calculated, and the statistical results are given in Figure 4. According to the figure, during the day time, the value of UHI intensity is negative, during the night time, the value is positive, indicating that the traffic volume in the downtown area at night is significantly higher than that during the day. Figure 5 shows the maximum UHI intensity and the distribution of its occurrence time and frequency, which reflected the distribution features of the environment temperature difference between the downtown and the suburb areas. According to the table, in the target city, the highest frequency of maximum UHI intensity is 3. Since the traffic roads cover a large area in the target city, the environment temperature difference between the downtown and the suburb areas is not that obvious; at the same time, evening and early

morning are the main occurrence time periods of maximum UHI intensity.

To investigate the relationship between UHI intensity and transportation energy consumption and carbon emission, this paper conducted correlation analysis and factor analysis on the UHI intensity and transportation energy consumption and carbon emission parameter samples, and the analysis results are listed in Table 1 and Table 2. According to the data in the tables, throughout the year and each season, in the target city, the UHI intensity is directly proportional to  $W_f$  and  $K$ , and inversely proportional to  $V$ ,  $\theta$ ,  $\varphi$ , and  $r$ , indicating that the key factors of UHI intensity are the height of the mixed layer in the urban thermal space and the wind speed. In addition, UHI intensity,  $W_f$ , and  $K$  are under a same factor; and  $V$ ,  $\theta$ ,  $\varphi$ , and  $r$  are under a same factor as well, indicating that parameters  $V$ ,  $\theta$ ,  $\varphi$ , and  $r$  have close internal relationships.

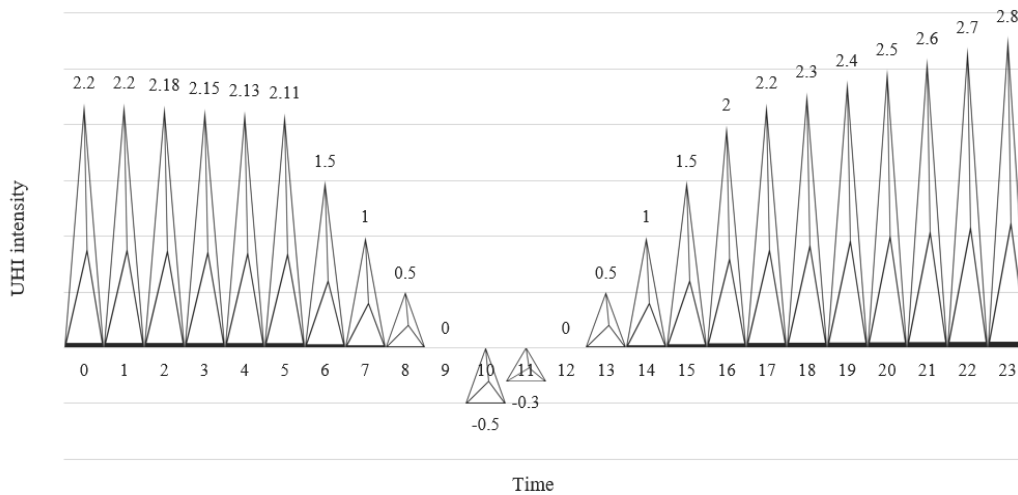


Figure 4. Daily changes of UHI intensity

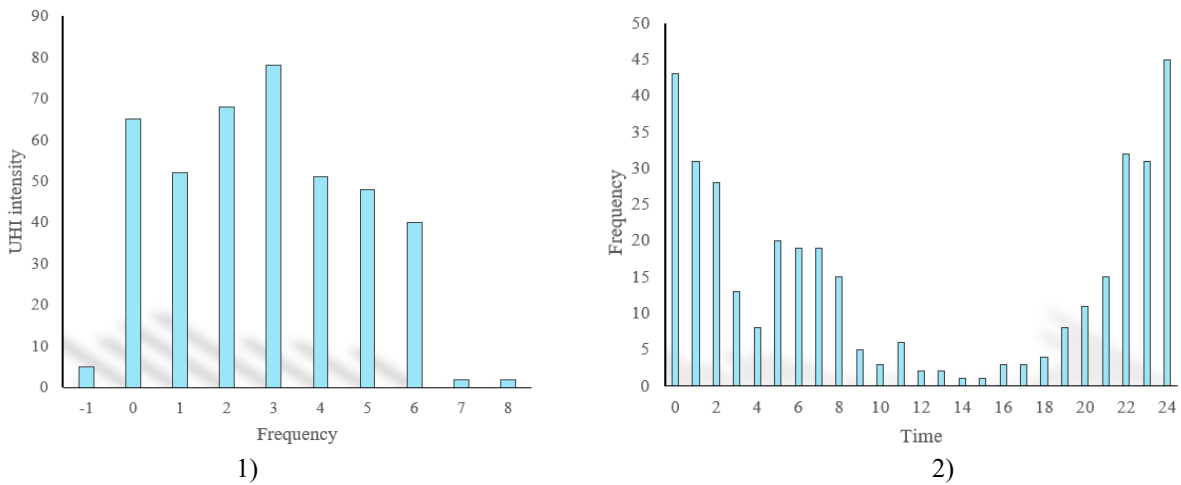


Figure 5. Maximum UHI intensity and the distribution of its occurrence time and frequency

Table 1. Correlation analysis results of UHI intensity

	$\theta$	$K$	$V$	$Q$	$\varphi$	$r$
Spring	-0.563**	-0.318**	-0.058*	0.035*	-0.048**	-0.037**
Summer	-0.547**	-0.372**	0.162**	-0.141**	-0.142**	0.069
Fall	-0.629**	-0.469**	-0.05	0.036	-0.062*	-0.027
Winter	-0.647**	-0.372**	0.157**	-0.269**	-0.037	0.261**
Year round	-0.539	-0.395**	0.063	-0.037	-0.059**	0.077

\*\* represents the significance level of  $P < 0.01$ ; \* represents the significance level of  $P < 0.05$ .

**Table 2.** Factor analysis results of UHI intensity

	<i>HHI</i>	$\theta$	<i>K</i>	<i>V</i>	<i>Q</i>	$\varphi$	<i>r</i>
Factor 1	0.048	0.02	0.169	0.958	-0.915	0.034	0.971
Factor 2	-0.827	0.615	0.748	0.062	-0.071	0.162	0.058
Factor 3	0.04	-0.629	0.043	-0.28	0.026	0.928	0.215

\*\* represents the significance level of  $P < 0.01$ ; \* represents the significance level of  $P < 0.05$ .

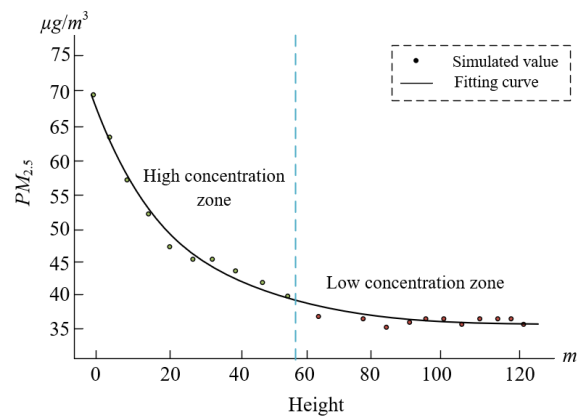
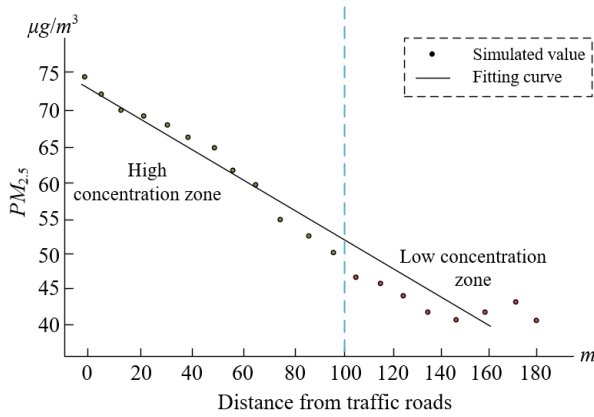


**Figure 6.** Horizontal distribution of average PM<sub>2.5</sub> concentration **Figure 7.** Vertical distribution of average PM<sub>2.5</sub> concentration

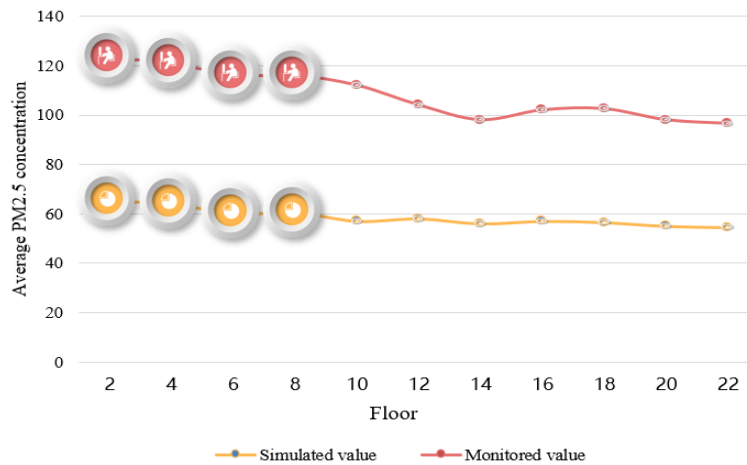


**Figure 8.** Comparison of monitoring and simulation results of average PM<sub>2.5</sub> concentration

Figures 6 and 7 give the trends of PM<sub>2.5</sub> concentration in the horizontal and vertical directions, showing the horizontal and vertical distribution of the average PM<sub>2.5</sub> concentration. The areas participated in the calculation were within the range of [0m, 180m] from urban traffic roads and within the range of [0m, 120m] above the urban ground surface. As can be seen from the figure, the PM<sub>2.5</sub> concentration within [0m, 100m] from urban traffic roads and within [0m, 58m] above urban ground surface was higher; while within [100m, 180m] from urban traffic roads and within [58m, 120m] above urban ground surface, the PM<sub>2.5</sub> concentration tended to be stable.

Figure 7 shows the vertical distribution of the average PM<sub>2.5</sub> concentration within the range of 0m-120m (0m < Z < 120m) above urban ground surface. Within the range of 0m < Z < 60m, the PM<sub>2.5</sub> concentration was higher and attenuated quickly from 73 µg/m<sup>3</sup> to 42 µg/m<sup>3</sup>. Within the range of Z > 60m, the PM<sub>2.5</sub> concentration changed between 40 µg/m<sup>3</sup> and 45 µg/m<sup>3</sup>. The overall distribution of the data was consistent with the trend of the exponential function, so the exponential function was adopted to fit the CFD data (error was less than 5%). With the gradient data as the indicator, the calculation areas were divided into two zones: the high PM<sub>2.5</sub>

concentration zone (HCA) within the area of 0m < Z < 60m, and the low PM<sub>2.5</sub> concentration zone (LCA) within the area of Z > 60m.

Figure 8 compares the monitoring results and simulation results of average PM<sub>2.5</sub> concentration in the urban thermal environment space caused by transportation energy consumption. As can be seen from the figure, with the increase of the floor number, the average PM<sub>2.5</sub> concentration decreased gradually, and the monitoring results and simulation results of average PM<sub>2.5</sub> concentration above the 14th floor tended to be stable, indicating that the urban thermal environment space above the 14th floor is less affected by the PM<sub>2.5</sub> concentration of urban traffic roads; in addition, the wind speed in the urban thermal environment space above the 14th floor is higher, so the dust particles are less likely to gather in this space.

## 5. CONCLUSION

This paper studied the urban thermal environment under the influence of transportation energy consumption and carbon

emission trend. At first, this paper gave the spatial structure of urban thermal environment, and constructed fluid flow control equation, heat transfer control equation, pollutant diffusion control equation, and turbulence model for the urban thermal environment. Then, this paper quantitatively analyzed the UHI intensity and air pollutant concentration, aiming to alleviate the UHI effect under the influence of transportation energy consumption and carbon emission trend. The experimental results summarized the daily changes of UHI intensity and gave the statistical results of the maximum UHI intensity and the distribution of its occurrence time and frequency, revealing the distribution features of the environment temperature difference between the downtown and the suburb areas. After that, this paper conducted correlation analysis and factor analysis on the UHI intensity and transportation energy consumption and carbon emission parameter samples and gave the analysis results, plotted the trends of PM<sub>2.5</sub> concentration in the horizontal and vertical directions, showing the horizontal and vertical distribution of the average PM<sub>2.5</sub> concentration. At last, this paper also compared the monitoring results and simulation results of average PM<sub>2.5</sub> concentration in the urban thermal environment space caused by transportation energy consumption.

#### ACKNOWLEDGMENT

This work is supported by Doctoral Research Start-up Fund Project, Linyi University (Grant No.: 18LUBK02).

#### REFERENCES

[1] Ježek, I., Blond, N., Skupinski, G., Močnik, G. (2018). The traffic emission-dispersion model for a Central-European city agrees with measured black carbon apportioned to traffic. *Atmospheric Environment*, 184: 177-190. <https://doi.org/10.1016/j.atmosenv.2018.04.028>

[2] Cong, R., Saito, M., Hirata, R., Ito, A., Maksyutov, S. (2018). Exploration on quantifying carbon dioxide (CO<sub>2</sub>) emission from road traffic in megacity. *International Archives of the Photogrammetry, Remote Sensing & Spatial Information Sciences*, 42(4): 185-192. <https://doi.org/10.5194/isprs-archives-XLII-4-115-2018>

[3] Hamdan, S., Jouini, O., Cheaitou, A., Jemai, Z., Alsyof, I., Bettayeb, M. (2019). Optimal air traffic Flow management with carbon emissions considerations. In *World Congress on Global Optimization*, pp. 1078-1088. [https://doi.org/10.1007/978-3-030-21803-4\\_106](https://doi.org/10.1007/978-3-030-21803-4_106)

[4] Blanco-Alegre, C., Calvo, A.I., Alves, C., Fialho, P., Nunes, T., Gomes, J., Fraile, R. (2020). Aethalometer measurements in a road tunnel: A step forward in the characterization of black carbon emissions from traffic. *Science of The Total Environment*, 703: 135483. <https://doi.org/10.1016/j.scitotenv.2019.135483>

[5] Peng, C., Fu, X., Gan, J., Xiang, Q. (2022). An estimation model of traffic carbon emission based on traffic planning index and STIRPAT in Counties. In *International Conference on Intelligent Transportation Engineering*, pp. 62-71. [https://doi.org/10.1007/978-981-19-2259-6\\_6](https://doi.org/10.1007/978-981-19-2259-6_6)

[6] Lv, Y., Li, X.J., Sun, H.J., Wang, X.R. (2022). Carbon neutrality based toll-subsidy design for road traffic

network under emission uncertainty. *System Engineering Theory and Practice*, 42(5): 1303-1313. <https://doi.org/10.12011/SETP2021-1311>

[7] Qi, S.N., Duan, M. (2022). Study on the impact of traffic carbon emission on environmental pollution considering time constraints. *Advances in Transportation Studies*, 1(S): 67-76. <https://doi.org/10.53136/97912599481137>

[8] Hao, C., Xin, Y. (2021). Decoupling analysis of traffic system carbon emission and coordination degree physical model. In *2021 3rd International Conference on Artificial Intelligence and Advanced Manufacture*, pp. 2620-2624. <https://doi.org/10.1145/3495018.3501152>

[9] Chen, W., Xiao, Z., Siming, Z. (2020). Low-carbon emission driven traffic speed optimization for internet of vehicles. In *International Conference on Edge Computing and IoT*, pp. 35-50. [https://doi.org/10.1007/978-3-030-73429-9\\_3](https://doi.org/10.1007/978-3-030-73429-9_3)

[10] Liao, J. (2021). Prediction method of urban traffic carbon emission reduction rate based on grey relational analysis. In *International Conference on Smart Transportation and City Engineering*, 12050: 637-643. <https://doi.org/10.1117/12.2614663>

[11] Li, Y., Li, T., Lu, S. (2021). Forecast of urban traffic carbon emission and analysis of influencing factors. *Energy Efficiency*, 14(8): 1-15. <https://doi.org/10.1007/s12053-021-10001-0>

[12] Chen, J., Liao, W., Yu, C. (2021). Route optimization for cold chain logistics of front warehouses based on traffic congestion and carbon emission. *Computers & Industrial Engineering*, 161: 107663. <https://doi.org/10.1016/j.cie.2021.107663>

[13] Niu, L., Pan, M., Xiong, L. (2020). Convergence analysis of urban green traffic carbon emission based on grey prediction model. *International Journal of Global Energy Issues*, 42(5-6): 285-301. <https://doi.org/10.1504/IJGEI.2020.111180>

[14] Huang, Y.H., Yan, Q.Y. (2020). Response to ‘Carbon emission flow from self-driving tours and its spatial relationship with scenic spots—A traffic-related big data method’. *Journal of Cleaner Production*, 247: 119540. <https://doi.org/10.1016/j.jclepro.2019.119540>

[15] Papp, B., Kristóf, G. (2020). The role of thermal convection in the dispersion of traffic-induced air pollutants in the Urban environment. *20th International Conference on Harmonisation within Atmospheric Dispersion Modelling for Regulatory Purposes*.

[16] Deng, Q., Zhou, Z., Li, C., Yang, G. (2022). Influence of a railway station and the Yangtze River on the local urban thermal environment of a subtropical city. *Journal of Asian Architecture and Building Engineering*, 21(2): 588-603. <https://doi.org/10.1080/13467581.2020.1845703>

[17] Yilmaz, S., Irmak, M.A., Qaid, A. (2022). Assessing the effects of different urban landscapes and built environment patterns on thermal comfort and air pollution in Erzurum city, Turkey. *Building and Environment*, 219: 109210. <https://doi.org/10.1016/j.buildenv.2022.109210>

[18] Zhou, H., Tao, G., Nie, Y., Yan, X., Sun, J. (2022). Outdoor thermal environment on road and its influencing factors in hot, humid weather: A case study in Xuzhou City, China. *Building and Environment*, 207: 108460. <https://doi.org/10.1016/j.buildenv.2021.108460>

- [19] Zheng, B., Li, J., Chen, X., Luo, X. (2022). Evaluating the effects of roof greening on the indoor thermal environment throughout the year in a Chinese city (Chenzhou). *Forests*, 13(2): 304. <https://doi.org/10.3390/f13020304>
- [20] Cai, Z., Tang, Y., Zhan, Q. (2021). A cooled city? Comparing human activity changes on the impact of urban thermal environment before and after city-wide lockdown. *Building and Environment*, 195: 107729. <https://doi.org/10.1016/j.buildenv.2021.107729>
- [21] Liu, Y., Li, H., Gao, P., Zhong, C. (2021). Monitoring the spatiotemporal dynamics of urban green space and its impacts on thermal environment in Shenzhen city from 1978 to 2018 with remote sensing data. *Photogrammetric Engineering & Remote Sensing*, 87(2): 81-89. <https://doi.org/10.14358/PERS.87.2.81>
- [22] Li, Y., He, J. (2021). Evaluating the improvement effect of low-energy strategies on the summer indoor thermal environment and cooling energy consumption in a library building: A case study in a hot-humid and less-windy city of China. In *Building Simulation*, 14(5): 1423-1437. <https://doi.org/10.1007/s12273-020-0747-6>
- [23] Chen, X., Yang, J., Zhu, R., Wong, M.S., Ren, C. (2021). Spatiotemporal impact of vehicle heat on urban thermal environment: A case study in Hong Kong. *Building and Environment*, 205: 108224. <https://doi.org/10.1016/j.buildenv.2021.108224>
- [24] Zhang, N., Ye, H., Wang, M., Li, Z., Li, S., Li, Y. (2022). Response relationship between the regional thermal environment and urban forms during rapid urbanization (2000–2010–2020): A case study of three urban agglomerations in China. *Remote Sensing*, 14(15): 3749. <https://doi.org/10.3390/rs14153749>
- [25] Baqa, M.F., Lu, L., Chen, F., Nawaz-ul-Huda, S., Pan, L., Tariq, A., Li, Q. (2022). Characterizing spatiotemporal variations in the urban thermal environment related to land cover changes in Karachi, Pakistan, from 2000 to 2020. *Remote Sensing*, 14(9): 2164. <https://doi.org/10.3390/rs14092164>